ELSEVIER

PII: S0032-3861(97)10122-7

Polymer Vol. 39 No. 25, pp. 6339–6346, 1998
© 1998 Elsevier Science Ltd
Printed in Great Britain. All rights reserved
0032-3861/98/$ - see front matter

Mixtures of polymer tails and loops grafted to an impenetrable interface

Daniel C. Driscoll[a], Harpreet S. Gulati[b,†], Richard J. Spontak[a,b,*] and Carol K. Hall[b]
[a]*Department of Materials Science & Engineering, North Carolina State University, Raleigh, NC 27695-7907, USA*
[b]*Department of Chemical Engineering, North Carolina State University, Raleigh, NC 27695-7907, USA*
(Received 27 June 1997; accepted 17 September 1997)

Property modification of an inorganic surface can be readily achieved through the use of macromolecules chemically grafted to the surface at specific functional sites along the chain. While numerous efforts have addressed the properties of linear chains grafted at one end (*tails*), relatively few have extended such studies to include double-tethered chains (*loops*). In this work, we consider loop/tail mixtures in which both chain species possess an identical number of repeat units. Bond-fluctuation simulations have been performed to ascertain the effects of composition, chain length and surface density on the segmental density distribution and layer height of each constituent species and of the mixture. These results compare favourably with self-consistent field predictions for bidisperse mixtures of grafted tails differing in length by a factor of two. © 1998 Elsevier Science Ltd. All rights reserved.

(Keywords: bond-fluctuation model; grafted polymers; brushes)

INTRODUCTION

Controlled modification of the properties of various impenetrable (primarily inorganic) surfaces can be readily accomplished through the use of grafted polymer chains. Grafted polymer chains are chemically attached to a surface at specific ('sticky') sites along the chain[1–3], and constitute a commercially viable means by which to customize surface properties to enhance, for example, adhesion[4], colloidal stabilization[5,6] and biocompatibility[7]. Precise property modification at nanometre length scales requires detailed information regarding the conformational characteristics of the grafted chains and the height of the resultant thin monolayer. While functional sites can, in principle, be chemically incorporated anywhere along the chain (see, for example, Ref. 8), one common approach has relied extensively on chain-end functionalization. More specifically, emphasis has been placed on chains capable of attaching to a surface at only one end. Such single-tethered chains are referred to as *tails*, and a concentrated layer of tails is designated a *brush*[9,10].

Over the past decade, polymer tails have remained the subject of extensive theoretical[6,11–19] and simulations[5,18,20–25] research, since studies of grafted tails provide valuable insight into the factors affecting chain conformation and packing within a highly constrained environment (i.e., within close proximity to a solid interface). Fundamental efforts addressing monodisperse and polydisperse grafted tails have also greatly assisted in elucidating the block and microdomain characteristics of microphase-ordered diblock copolymers and copolymer mixtures[26–30]. Topics of particular interest in static tail and brush analyses generally include equilibrium chain conformations and packing, as described in terms of the chain gyration radius (R_g), the segmental density profile normal to the interface (ρ_z) and the polymer layer thickness (h). Scaling relationships are also of considerable value in such investigations, since they not only distinguish between different conformational regimes, but also facilitate the design of grafted polymer layers from limited experimental data. For instance, h in a good solvent is predicted[11,12] to scale as $N\sigma^{1/3}$, where N is the number of repeat units in the chain and σ denotes the density of anchored sites. Likewise, the critical impingement density (σ_c), the density at which neighboring chains interact and are forced away from the surface due to increased volume exclusion, varies as $N^{-6/5}$ for tails.

If both ends of a chain are chemically functionalized, then the chain upon grafting is more highly constrained, tethered to the surface at two sites and forming a polymer *loop*. The conformational[31–33] and dynamic[33,34] properties of loops have also been examined, but not nearly to the same extent as tails. One reason for this is that looped chains have been conventionally regarded as tails of half chain length. This assumption accurately describes the extension of looped blocks in microphase-ordered block copolymers[35–38], and prior bond-fluctuation (BF) simulations[32] reveal that the critical chain impingement density for loops obeys the same scaling relationship as that for tails. However, discontinuous molecular dynamics (DMD) simulations[33,34] have shown that the scaling relationships describing the lateral diffusivity and relaxation time of polymer loops differ substantially from those of polymer tails. Moreover, segmental density profiles of loops exhibit greater chain stretching than tails at comparable surface anchor densities. Thus, while loops may be envisaged as tails of half chain length at low σ and N, their conformational and dynamic characteristics may deviate from those of tails when density saturation effects become non-negligible.

* To whom correspondence should be addressed
† Present address: Simulation Sciences Inc., 601 Valencia Ave., Suite 100, Brea, CA 92823, USA

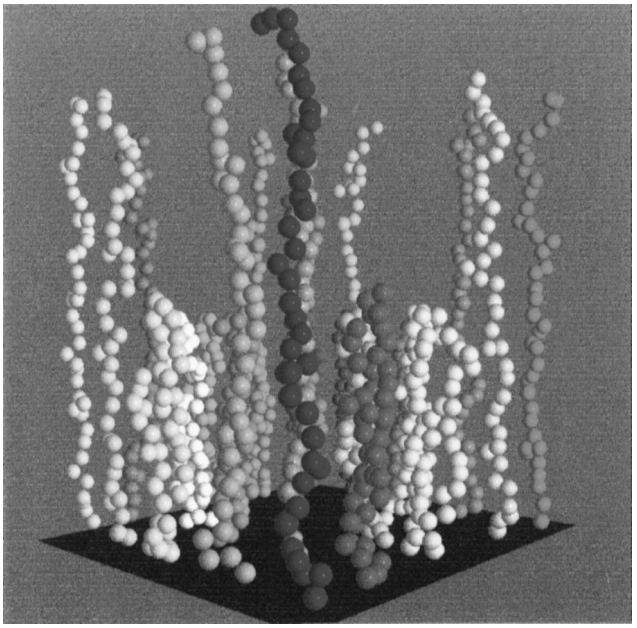

Figure 1 Discontinuous molecular dynamics (DMD) snapshot of a binary mixture of single- and double-grafted polymer chains (*tails* and *loops*, respectively) at an impenetrable interface. This snapshot shows the chains in their near-initial bond-fluctuation (BF) simulation conformation for the sake of clarity. Note that both chain species contain the same number of repeat units ($N = 40$)

While systems consisting of either tails or loops at constant N have been previously investigated (to different extents), relatively little has been reported regarding the conformational characteristics[14,16–19] and phase behaviour[39,40] of binary loop or tail mixtures (each containing two isoconformational chain species differing in N), let alone a mixture of loops *and* tails grafted to an impenetrable interface. In addition to describing a mixture of dual-end-functionalized loops and single-end-functionalized tails of equal N (illustrated in *Figure 1*), a loop/tail mixture is likewise applicable to the case of dual-end-functionalized chains in which only some of the chains successfully re-enter the layer to attach to the interface and consequently form loops[41]. The objectives of the present work are two-fold: (i) to ascertain the effects of varying N, σ and mixture composition on the equilibrium conformational and layer characteristics of grafted loop/tail mixtures through the use of BF simulations, and (ii) to compare conformational and layer characteristics of such mixtures to those of an analogous bidisperse mixture of grafted tails differing in N by a factor of two.

SIMULATION ALGORITHM

The BF model, described in detail elsewhere[32,42,43], was used to simulate mixtures of single- and double-tethered chains at an impenetrable surface in the presence of a good solvent. The 3D periodic cell used in these simulations consisted of 50×50 lattice parameters, and the cell height was larger than the length of the longest chain fully extended along the $+z$ direction (normal to the interface). The BF model is an on-lattice Monte Carlo algorithm that allows both bond length and direction to fluctuate according to the following restrictions: bond lengths must lie within 2 to $\sqrt{10}$ lattice parameters, and bond vectors are limited to the set {(2,0,0), (2,1,0), (2,1,1), (2,2,1), (3,0,0), and (3,1,0)} and all permutations thereof. Due to flexibility in bond length and direction, the BF model comes close to emulating off-lattice simulations, although subtle differences remain[33,43].

At the onset of each simulation, the graft sites of the loops and tails are randomly placed inside the periodic cell at equally spaced positions, the distance between which depends on the number of chains employed in the simulation, which, in turn, depends on the chosen surface density (σ). The surface density, in conjunction with the blend composition, also dictates the size of the system, which ranged from 9 to 100 chains of length (N) 20, 40 and 60 in this study. As described in detail elsewhere[32], the polymer chains are initially arranged in an extended conformation normal to the surface at $z = 0$. Accordingly, tails start as straight chains of N beads perpendicular to the surface, while loops begin as hairpins of N beads (i.e., $N/2$ beads comprise the sides of the hairpin normal to the surface and connect at the top by a single bond of length 2). The grafted sites remain stationary during system initialization, but are subsequently allowed to diffuse laterally along the surface during system relaxation and simulation to eliminate any memory of their initial placement. The BF simulation proceeds by first selecting a random bead on a random chain and then moving the bead at that position by one step in a random direction. The move is accepted if: (i) the resulting bond vector remains in the set listed above, and (ii) the site selected is not occupied by another bead (including its neighboring sites). Equilibrium is achieved in the simulations reported here by adhering to the protocol established earlier[32] for polymer loops of constant N grafted to an impenetrable interface (this protocol averages three independent simulation runs and assures virtually constant chain and layer characteristics).

RESULTS AND DISCUSSION

Segmental density distributions for loops ($\rho_{z,l}$) and tails ($\rho_{z,t}$) in which $\int_0^\infty \rho_{z,i} dz = 1$ (i = l or t) and $N = 40$ are shown in *Figure 2* for loop mole fractions (x_l) of 0.00, 0.25, 0.50, 0.75 and 1.00 at a surface density (σ) of 0.11. (Since a loop is grafted at two sites/chain, while each tail is anchored at only one end, surface density is defined here in terms of the number of chains, *not* graft sites, per unit area.) Under these conditions, adjacent loops and/or tails are expected to interact with one another by excluding available volume, since the critical impingement density ($\sigma_c \approx 0.03$ for a layer composed solely of looped chains[32]) is exceeded. When $\sigma < \sigma_c$, isolated grafted chains (loops or tails) adopt a mushroom-like conformation since no volume constraints exist. At higher σ ($> \sigma_c$), within the 'scaling' regime, however, the layer densifies as the constituent chains become laterally compressed. In this regime, the segmental density distribution of either tails or loops normal to the surface is predicted[6,13,14] to follow a parabolic trajectory. Such distributions are evident in *Figure 2a* for pure loops ($\rho_{z,l}$ at $x_l = 1.00$) and in *Figure 2b* for pure tails ($\rho_{z,t}$ at $x_l = 0.00$). As x_l increases from 0.25 to 1.00 in *Figure 2a*, two characteristics of the resulting $\rho_{z,l}$ warrant attention: the maximum density near $z = 0$ decreases nonlinearly, whereas the average loop extension (along z) increases. These observations reveal that, in the presence of single-grafted tails, the double-tethered loops are forced to reside closer to the surface than do loops in the absence of tails.

According to *Figure 2b*, the shapes of the $\rho_{z,t}$ distributions depend more sensitively on mixture composition than the shapes of the $\rho_{z,l}$ distributions (*Figure 2a*). As the fraction of loops is increased from 0.00 to 0.75, the parabolic profile representative of a layer composed only of tails transforms into profiles exhibiting a peak density along z in the vicinity

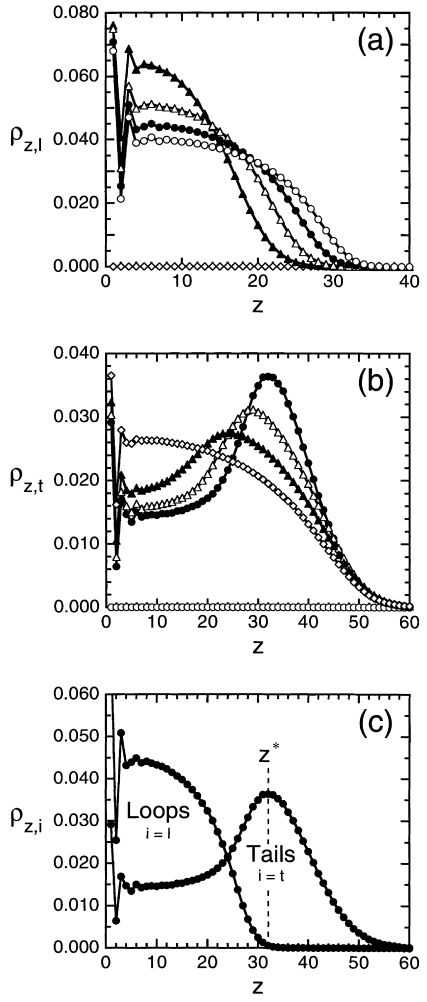

Figure 2 Segmental density distributions for (a) polymer loops ($\rho_{z,l}$) and (b) tails ($\rho_{z,t}$) for five mixtures with different loop fractions (x_l): 1.00 (○), 0.75 (●), 0.50 (△), 0.25 (▲) and 0.00 (◇). In (c), the loop and tail segmental density distributions for one mixture ($x_l = 0.75$) are presented together for direct comparison. Also labelled in (c) is z^* for the $x_l = 0.75$ mixture. In each case, $N = 40$ and $\sigma = 0.11$. The solid lines serve as guides for the eye

where the corresponding $\rho_{z,l}$ vanishes. Moreover, the magnitude and position of these peak densities (relative to the interface at $z = 0$) both increase with increasing loop concentration. These profile characteristics indicate that, upon increasing x_l, the tails are effectively forced away from the interface due to loop-induced volume exclusion and adopt a more highly extended conformation along the interface normal. Since the tails must adopt a stretched (entropically unfavourable) conformation near the interface, they squeeze the loops closer to the interface, which explains the composition-induced loop compression evident in the $\rho_{z,l}$ distributions discussed above (*Figure 2a*).

Spatial competition between loops and tails consequently appears to result in the formation of two sublayers: a dense inner sublayer composed of both loops and tails in close proximity to the interface, and a boundary sublayer consisting primarily of tails at z beyond the inner sublayer. Similar layering is predicted[16–19] for bidisperse mixtures of tails grafted to an impenetrable interface. To facilitate visualization of these distinct sublayers, the $\rho_{z,l}$ and $\rho_{z,t}$ distributions for the mixture possessing 75% loops are presented together in *Figure 2c*. Note that, in this figure, $\rho_{z,t}$ is relatively invariant with respect to position up to $z \approx 20$ and the maximum in $\rho_{z,t}$ occurs at almost the same z as that

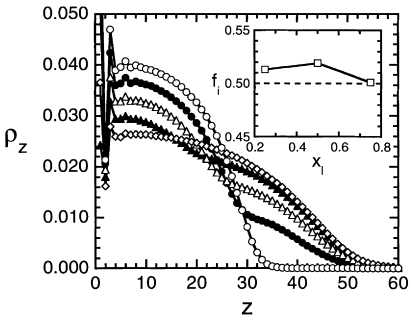

Figure 3 The total segmental density distributions (ρ_z) for the polymer layers corresponding to the distributions presented in *Figure 2* (using the same symbols). The inset displays the fraction of segments residing in the loop-rich inner sublayer (f_i) for the three mixtures examined here. The solid lines serve as guides for the eye

at which $\rho_{z,l}$ approaches zero. At distances beyond this z, $\rho_{z,t}$ decays according to a parabolic trajectory so that the tail segments comprising the boundary sublayer adopt a more unperturbed (relaxed) conformation along z than those stretched segments restricted to the inner sublayer. For the mixture used to generate *Figure 2c*, the looped chains can therefore be pictured as flattened mushrooms, while the tails appear as interspersed long-stemmed broccoli.

The total segmental density profiles (ρ_z) associated with the loop/tail mixtures shown in *Figure 2* are provided in *Figure 3*. Each profile is the mole fraction average of $\rho_{z,l}$ and $\rho_{z,t}$ normalized so that $\int_0^\infty \rho_z \, dz = 1$. The formation of a structurally tiered monolayer becomes evident in these distributions when the simple parabolic shape of ρ_z (for pure loops or pure tails) evolves into a profile exhibiting a kink, which occurs for all of the mixtures examined here. Recall that the layer with the highest ρ_z near the surface (at $z = 0$) consists of looped chains, reflecting the added conformational constraint of a second graft site. On the basis of similar considerations, the boundary layer residing farther from the surface is rich in tails. As the fraction of tails in the mixtures is increased from 0.25 ($x_l = 0.75$) to 0.75 ($x_l = 0.25$), it is reasonable to expect a proportional reduction in ρ_z near the surface, since fewer chains possess two graft sites. The results displayed in *Figure 3* are consistent with this expectation. Also shown in the inset of *Figure 3* is the fraction of segments residing in the inner loop-rich sublayer for the three loop/tail mixtures discussed thus far. This fraction, denoted f_i, is calculated from

$$f_i = \frac{\int_0^{z^*} \rho_z \, dz}{\int_0^{\infty} \rho_z \, dz} \tag{1}$$

where z^* is the position along z where $\rho_{z,t}$ exhibits a maximum and $\rho_{z,l}$ approaches zero (identified in *Figure 2c*). Since $\int_0^\infty \rho_z \, dz = 1$, the fraction of segments in the outer boundary layer (f_b) can be immediately obtained from $1 - f_i$. From the inset in *Figure 3*, it can be concluded that f_i remains relatively constant at ≈ 0.5, and is therefore not strongly dependent on the fraction of loops, for the three mixture compositions examined here.

Shown in *Figure 4* are extremum density profiles for loops and tails in the same mixtures described in *Figures 2* and *3* (with $N = 40$ and $\sigma = 0.11$). Here, *extremum* refers to the two median beads (located at positions $N/2$ and $N/2 + 1$) on looped chains and the end bead (located at N) on tails. According to the data in *Figure 4a*, the median bead density

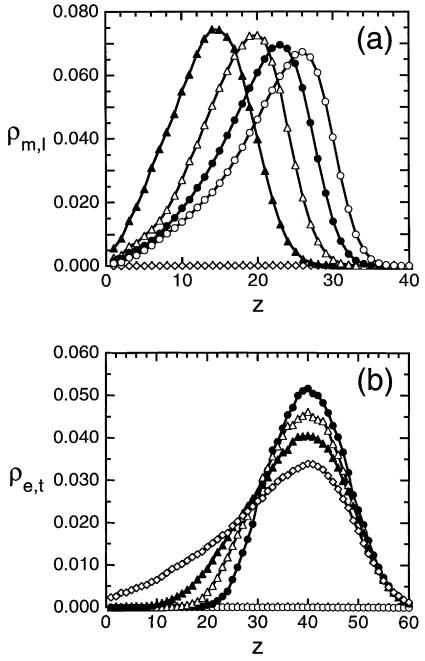

Figure 4 Extremum density distributions of (a) the two median beads on looped chains and (b) the end bead on tails for the mixtures described in *Figure 2* (using the same symbols). The solid lines are guides for the eye

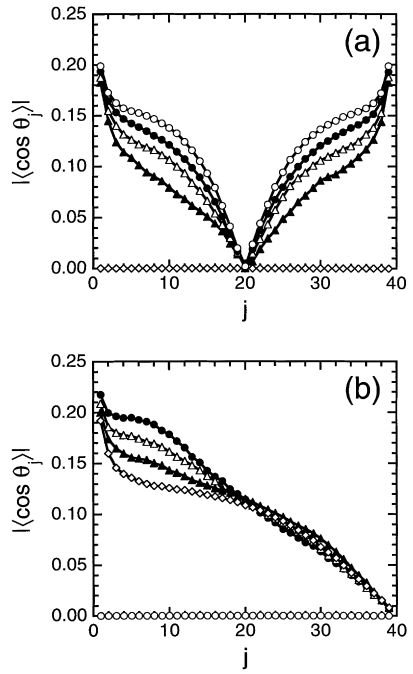

Figure 5 Local stretching of the grafted (a) loops and (b) tails, as discerned from the absolute mean projection of the *j*th bond vector normal to the interface ($|\langle\cos\theta_j\rangle|$), for the mixtures described in *Figure 2* (using the same symbols). The solid lines serve as guides for the eye

profiles for the loops ($\rho_{m,l}$) are asymmetric when only loops are present ($x_l = 1.00$). For a layer composed solely of looped chains, this feature indicates that most of the median beads lie near the outer surface of the layer due to volume exclusion considerations. As x_l decreases and the looped chains are squeezed toward the surface, the position corresponding to the maximum in $\rho_{m,l}$ is seen to shift toward $z = 0$, and the shape of the distribution becomes more symmetric about its maximum.

In marked contrast, the shapes of the end-bead density profiles for the tails ($\rho_{e,t}$) depend more sensitively on mixture composition, as seen in *Figure 4b*. When the layer is composed of only tails, the corresponding end bead profile also appears highly asymmetric, exhibiting an onset at the interface position (at $z = 0$) and a maximum at a position along z near the outermost surface of the polymer monolayer (where ρ_z in *Figure 3* approaches zero). As the concentration of loops is increased, however, the magnitude, but *not* the position, of the maximum is observed to increase, while the onset of the distribution shifts outward (along z) from the interface. This shift in the onset of the tail end distributions in loop/tail mixtures reveals that the probability of finding the end of a tail near the surface is diminished substantially in the presence of an inner sublayer consisting of looped chains. Such behaviour can have commercial ramifications if the mixture under consideration is formed by sequential dual-end-functionalized grafting, in which case both ends of each chain attach in turn to the surface[41]. From the results presented in *Figure 4a* and *Figure 4b*, it is clear that the probability of forming loops from polymer chains functionalized with sticky sites at both ends decreases markedly as the concentration of loops increases.

Local stretching of individual bond vectors can be quantified through the cosine of the angle between the *j*th bond vector and the direction normal to the surface; i.e., $(z_{j+1} - z_j)/(|\mathbf{r}_{j+1} - \mathbf{r}_j|)$, where $\mathbf{r}_j$ is the positional vector of the *j*th repeat unit and $\mathbf{z}_j$ corresponds to the normal component of the positional vector. Since this ratio, denoted as $\cos\theta_j$, increases as the chains extend away from the interface and the bonds consequently align normal to the interface, it constitutes an excellent measure of local chain stretching within the mixed inner sublayer. Shown in *Figure 5* is the absolute mean projection of the *j*th bond vector normal to the interface, denoted $|\langle\cos\theta_j\rangle|$, as a function of bond position j along the chain backbone for polymer loops (*Figure 5a*) and tails (*Figure 5b*) with $N = 40$ and $\sigma = 0.11$. As the concentration of loops in the loop/tail mixture decreases and the loop-rich inner sublayer becomes increasingly more compressed along the interface normal (i.e., squeezed toward the surface), the loops cannot extend freely from the interface, resulting in a reduction in $|\langle\cos\theta_j\rangle|$ with decreasing x_l, as seen in *Figure 5a*. In similar fashion, $|\langle\cos\theta_j\rangle|$ for the tails within the inner sublayer are observed in *Figure 5b* to decrease initially (for $j < 20$) as the loop fraction decreases. At high x_l, the tails residing in the inner sublayer are forced to adopt a more locally extended conformation due to lateral chain compression, resulting in an increase in $|\langle\cos\theta_j\rangle|$. Within the outer tail-rich boundary sublayer ($j > 20$), however, mixture composition appears to have very little effect on local tail stretching, according to the BF results displayed in *Figure 5b*. This observation implies that the local stretching of the part of a tail residing in the tail-rich boundary sublayer is not greatly affected by the enhanced stretching of the part of the tail within the loop-rich inner sublayer. Thus, the local stretching of the tail fraction within the boundary sublayer can be considered, to a first approximation, independent of the inner sublayer.

The simulation results presented thus far illustrate how the segmental density and bond orientation distributions of polymer loops and tails vary with blend composition at fixed N (= 40) and σ (= 0.11). In this section, we explore the dependence of chain/layer properties on composition, chain length and surface density. Displayed in *Figure 6* is the composition dependence of the first moment of the

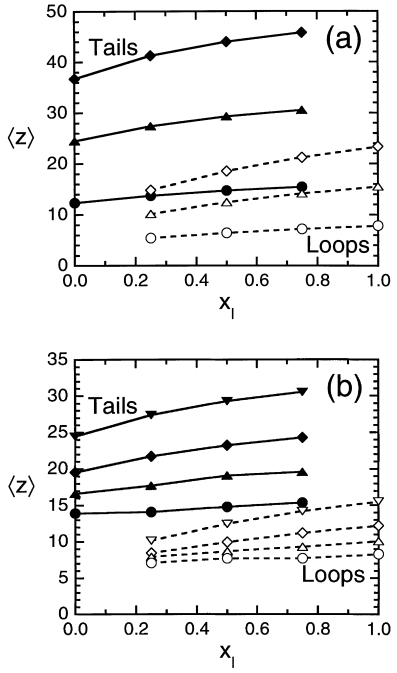

Figure 6 Average layer heights (⟨*z*⟩) of the loop (open symbols) and tail (filled symbols) sublayers provided as a function of mixture composition (x_l) for the cases of (*a*) $\sigma = 0.16$ and (*b*) $N = 40$. In (a), three values of *N* are examined: 20 (circles), 40 (triangles) and 60 (diamonds). In (b), four values of σ are shown: 0.06 (circles), 0.08 (triangles), 0.10 (diamonds) and 0.16 (inverted triangles). The solid and dashed lines for tails and loops, respectively, are guides for the eye

segmental density profile, denoted ⟨*z*⟩, which is an established measure of the polymer layer height (*h*). It is defined by

$$\langle z \rangle = \frac{\int_0^\infty z\rho_z(z)\,\mathrm{d}z}{\int_0^\infty \rho_z(z)\,\mathrm{d}z} \qquad (2)$$

In *Figure 6a*, ⟨*z*⟩ is provided as a function of x_l for both polymer loops and tails of varying chain length ($N = 20$, 40 and 60) at $\sigma = 0.16$. It is immediately apparent from this figure that an increase in *N* results in an increase in ⟨*z*⟩ of both the loop and tail constituents due to conservation of mass. Another feature of this figure is that ⟨*z*⟩ appears to increase monotonically with increasing x_l at constant *N*. This trend can be explained in terms of chain packing when we consider two different modes of chain compression that compete as x_l is increased: (1) *lateral* compression due to an increase in effective surface density, and (2) *normal* compression due to an increase in the entropically unfavourable stretching of tails. As x_l is increased, compression of the loops within the inner sublayer along the interface normal is gradually alleviated, allowing the loops to extend and fill space as they would ordinarily, in the absence of tails. Loop extension also increases in this case due to more lateral chain compression arising from impingement of neighboring loops. The tails, on the other hand, are forced to stretch further away from the interface as x_l and, consequently, the height of the loop-rich inner sublayer increases, as reflected by the increase in ⟨*z*⟩ for the tails in *Figure 6a*. *Figure 6a* also reveals that this relationship between ⟨*z*⟩ and x_l for both loops and tails becomes more pronounced as *N* becomes larger. In *Figure 6b*, the variation of ⟨*z*⟩ with respect to x_l and surface density (σ) at constant *N* is

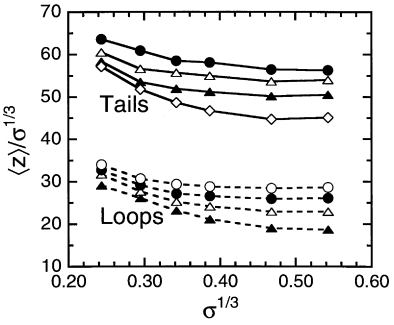

Figure 7 Variation of the reduced average layer height ($\langle z\rangle/\sigma^{1/3}$) with $\sigma^{1/3}$ for tails (top) and loops (bottom) at different loop fractions (x_l): 1.00 (○), 0.75 (●), 0.50 (△), 0.25 (▲) and 0.00 (◇). The critical impingement density is exceeded (and the scaling regime entered) when $\langle z\rangle/\sigma^{1/3}$ becomes independent of $\sigma^{1/3}$. The solid and dashed lines for tails and loops, respectively, serve as guides for the eye

presented. Here, ⟨*z*⟩ is seen to increase substantially with increasing σ at constant x_l and, to a lesser extent (especially at low σ), with increasing x_l at constant σ. These trends can again be attributed to chain packing considerations, since an increase in σ will generally induce greater chain stretching away from the interface due to the increase in excluded volume upon layer densification.

According to the predictions of classical self-consistent field (SCF) theory[13] for a polymer brush (i.e., a concentrated layer of tails), ⟨*z*⟩ scales as $N\sigma^{1/3}$. Recent DMD simulations have demonstrated[33] that, at constant *N*, polymer loops grafted to an impenetrable interface obey this relationship within the 'scaling' regime. Shown in *Figure 7* is $\langle z\rangle/\sigma^{1/3}$ as a function of $\sigma^{1/3}$ for each of the loop/tail mixtures examined in the previous sections (with *N* held constant at 40). Scaling behaviour is observed in this figure when $\langle z\rangle/\sigma^{1/3}$ is independent of $\sigma^{1/3}$, which occurs at relatively large σ for both loops and tails at all mixture compositions. Below the onset of the scaling threshold (where $\sigma < \sigma_c$), $\langle z\rangle/\sigma^{1/3}$ varies with $\sigma^{1/3}$ since ⟨*z*⟩ is nearly independent of σ, indicating that interchain interactions are virtually absent. Each chain therefore behaves as a random coil, adopting a mushroom-like conformation, and ⟨*z*⟩ only depends on *N*.

An alternative method for establishing the 'scaling' regime for grafted polymer chains is through the use of the normal component of the radius of gyration (R_{gz}), which is another measure of chain extension along the interfacial normal and which is also proportional to the layer height (*h*). *Figure 8* displays $R_{gz}/N\sigma^{1/3}$ *versus* $N\sigma^{1/3}$ for chains with different *N* at a single mixture composition ($x_l = 0.50$). The mixture exhibits scaling behaviour when $R_{gz}/N\sigma^{1/3}$ for both loops and tails is not dependent on $N\sigma^{1/3}$. The onset of the scaling regime in this figure appears to occur at larger values of $N\sigma^{1/3}$ as *N* is increased. Also provided for comparison in *Figure 8* are results obtained from pure loops and pure tails with $N = 40$. It is important to recognize that $R_{gz}/N\sigma^{1/3}$ for the pure tails is less than that for the tails in the 50/50 loop/tail mixture, revealing that the tails in the mixture are stretched further away from the interface. Conversely, since $R_{gz}/N\sigma^{1/3}$ for the pure loops is greater than that of the loops in the 50/50 mixture, it can be concluded that the looped chains in the mixture are compressed, lying closer to the interface than they normally would due to the presence of tails.

Since loops are often considered as tails of half chain length, we have elected to compare the BF simulation results obtained here for loop/tail mixtures with SCF

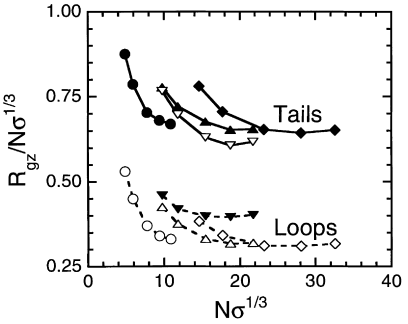

Figure 8 Reduced average layer heights for loops and tails, expressed in terms of $R_{gz}/N\sigma^{1/3}$, as a function of $N\sigma^{1/3}$ for one mixture ($x_l = 0.50$) and three different N: 20 (○, loops; ●, tails), 40 (△, loops; ▲, tails) and 60 (◇, loops; ◆, tails). The tails and loops exhibit scaling behaviour when $R_{gz}/N\sigma^{1/3}$ is independent of $N\sigma^{1/3}$. Also shown for comparison are values of $R_{gz}/N\sigma^{1/3}$ for pure loops (▼) and tails (▽) with $N = 40$. The solid and dashed lines are provided as guides for the eye

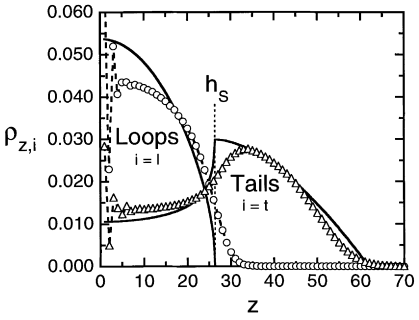

Figure 9 Comparison of segmental density distributions for loops ($\rho_{z,l}$, ○) and tails ($\rho_{z,t}$, △) from BF simulations and SCF predictions (equations (3a) and (3b)) for a bidisperse mixture of short ($\rho_{z,S}$) and long ($\rho_{z,L}$) tails differing in length by a factor of two (solid lines). In this case, $N = 40$, $\sigma = 0.16$ and $x_l = 0.50$. The dashed lines connect the simulation results and are guides for the eye

predictions for a bidisperse mixture of tails of lengths N_L and N_S, where $N_L = 2N_S$ and the subscripts refer to long (L) and short (S) tails. The SCF theoretical framework chosen for this comparison is that proposed by Lai and Zhulina[18]. Following their derivation, α accounts for chain length disparity and is defined as $(N_L - N_S)/N_S$. In the present analysis of loop/tail mixtures, $\alpha = 1$ for all cases. Since each looped chain corresponds to two short tails, the equivalent SCF surface density (σ_{eq}) is given by $\sigma(1 + x_l)$. It immediately follows that the fraction of short chains (x_S) in the equivalent bidisperse tail mixture is $2x_l/(1 + x_l)$, and the corresponding fraction of long chains (x_L) is $1 - x_S$. The SCF-predicted segmental density profiles for the long and short tails ($\rho_{z,S}$ and $\rho_{z,L}$, respectively) are

$$\rho_{z,S}(z) = \frac{3}{\pi}\sigma_{eq}^{2/3}\left(\frac{\pi^2 a^3}{8pv}\right)^{1/3}\left[x_L^{1/3}\sqrt{1 - x_L^{2/3} - z_r^2} + (1 - z_r^2) \times \tan^{-1}\left(\frac{\sqrt{h_S^2 - z^2}}{h_o x_L^{1/3}}\right)\right] \quad (3a)$$

$$\rho_{z,L}(z) = \begin{cases} \rho_z(z) - \rho_{z,S}(z) & 0 \le z \le h_S \\ \rho_z(z) & h_S \le z \le h_L \end{cases} \quad (3b)$$

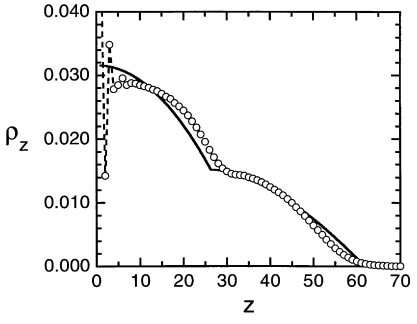

Figure 10 Comparison of the total segmental density distributions from BF simulations (○) and SCF theory (equation (4)) for a bidisperse mixture of short and long tails differing in length by a factor of two (solid line). As in *Figure 9*, $N = 40$, $\sigma = 0.16$ and $x_l = 0.50$. The dashed line connects the simulation results and serves as a guide for the eye

where

$$\rho_z(z) = \begin{cases} \frac{3}{2}\sigma_{eq}^{2/3}\left(\frac{\pi^2 a^3}{8pv}\right)^{1/3}[1 - z_r^2] & 0 \le z \le h_S \\ \frac{3}{2}\sigma_{eq}^{2/3}\left(\frac{\pi^2 a^3}{8pv}\right)^{1/3}[1 - u^2(z_r)] & h_S \le z \le h_L \end{cases} \quad (4)$$

Molecular properties referred to in equations (3) and (4) and equation (4) include the monomer length (a), the chain stiffness parameter (p) and the second virial coefficient (v). Values of a and the product pv used in the SCF calculations that are compared with the BF simulation results obtained here are, according to the results of Lai and Zhulina[18,24], 2 and 31.2, respectively. The sublayer heights employed in these equations (h_k, k = S or L) are given by

$$h_S = h_o(1 - x_L^{2/3})^{1/2} \quad (5a)$$

$$h_L = h_o(1 + \alpha x_L^{1/3}) \quad (5b)$$

where $h_o = (8pv\sigma_{eq}/\pi^2)^{1/3}N_S$. Lastly, z_r is defined as z/h_o, and the function $u(z_r)$ is evaluated from

$$u(z_r) = \frac{z_r - \alpha[z_r^2 - (1 - \alpha^2)(1 - x_L^{2/3})]^{1/2}}{1 - \alpha^2} \quad (6)$$

Predictions for $\rho_{z,S}$, $\rho_{z,L}$ and ρ_z based on this SCF theoretical framework for a mixture of bidisperse grafted tails (with $\alpha = 1$) are compared to BF simulations in *Figure 9* (individual segmental density distributions) and *Figure 10* (total segmental density distribution) for a single mixture in which $N = 40$, $\sigma = 0.16$ ($\sigma_{eq} = 0.11$) and $x_l = 0.50$ ($x_L = 0.33$). It is clear from both of these figures that the SCF predictions for the bidisperse tail mixture agree very well with the BF simulations obtained here for the grafted loop/tail mixture. The principal difference between the SCF predictions and BF simulations in *Figure 9* appears to be a sharp demarcation at h_S in the SCF formalism. This predicted feature is a consequence of the assumption made in the formalism that the constituent chains completely demix (which is only rigorously true in the limit of infinitely long chains). It is important to note that the SCF predictions in *Figure 10* correctly show a kink in $\rho_z(z)$ in the vicinity of $z \approx 26$, which corresponds to the crossover from the inner sublayer to the boundary sublayer.

In addition to the segmental density distributions shown in *Figures 9* and *10*, the extremum density profiles (i.e. the distribution functions of the two median beads in looped chains and the end bead in tails) obtained from BF

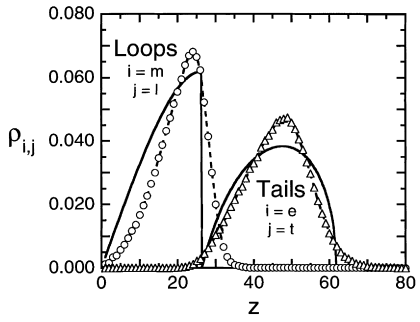

Figure 11 Comparison of the extremum density distributions for the two median beads on looped chains ($\rho_{m,l}$) and for the end bead on tails ($\rho_{e,t}$) with SCF predictions (equations (7) and (7)) for the end bead of each tail species in a bidisperse mixture of short and long tails differing in length by a factor of two (solid lines). The symbols and conditions are the same as those used in *Figure 9*

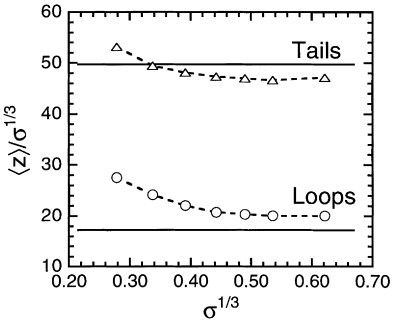

Figure 12 Reduced average layer height $\langle z\rangle/\sigma^{1/3}$ as a function of $\sigma^{1/3}$ for the same mixture as is described in *Figure 9* (using the same symbols for the simulation results). The dashed lines are guides for the eye, but the solid lines correspond to SCF predictions (equations (8) and (8)) for a bidisperse mixture of short and long tails differing in length by a factor of two

simulations and SCF predictions are also compared here. According to Lai and Zhulina[18], the functions for these profiles ($\rho_{e,S}$ and $\rho_{e,L}$, respectively) in a bidisperse tail mixture are

$$\rho_{e,S}(z) = \frac{3z\sqrt{h_o^2 - z^2}}{(1-x_L)h_o} \quad 0 \le z \le h_S \tag{7a}$$

$$\rho_{e,L}(z) = \frac{3u(z_r)\sqrt{1-u^2(z_r)}}{x_L(1-\alpha^2)h_o}\left[1 - \frac{\alpha z}{\sqrt{z^2-(1-\alpha^2)h_S^2}}\right]$$

$$h_S \le z \le h_L \tag{7b}$$

Figure 11 reveals that the SCF predictions produced with equations (7a) and (7b) are again in good agreement with the BF simulations for the median (loop) profile ($\rho_{m,l}$) and the end (tail) profile ($\rho_{e,t}$) obtained for the same mixture as is discussed in *Figures 9* and *10*. As in *Figure 9*, the primary difference between the simulated values for $\rho_{m,l}$ and $\rho_{e,t}$ and the predicted values for $\rho_{e,S}$ and $\rho_{e,L}$ in *Figure 11* is the sharp demarcation between the sublayer boundaries that results from the SCF formalism. In contrast, the BF simulations in *Figures 9* and *11* are seen to exhibit smoother, more diffuse boundaries.

Expressions for the heights of the inner and boundary sublayers in a bidisperse tail mixture have also been derived by Lai and Zhulina[18] in terms of the first moment of the segmental density profiles ($\langle z\rangle$):

$$\langle z\rangle_S = \frac{3h_o}{4\pi(1-x_L)} \times \left[(x_L^{1/3} - 2x_L)\sqrt{1-x_L^{2/3}} + \tan^{-1}\left(\frac{\sqrt{1-x_L^{2/3}}}{x_L^{1/3}}\right)\right] \tag{8a}$$

$$\langle z\rangle_L = \frac{3h_o}{8x_L(1+\alpha)}\left[1 + \alpha x_L^{1/3} + \alpha x_L + \alpha^2 x_L^{4/3} + \frac{\alpha(1-x_L^{2/3})^2}{2} \times \ln\left(\frac{1-x_L^{1/3}}{1+x_L^{1/3}}\right)\right] - \frac{(1-x_L)\langle z\rangle_S}{x_L(1+\alpha)} \tag{8b}$$

Figure 12 displays $\langle z\rangle/\sigma^{1/3}$ as a function of $\sigma^{1/3}$ for mixtures with $N = 20$ and $x_l = 0.50$. As seen earlier in *Figure 7*, $\langle z\rangle/\sigma^{1/3}$ for both loops and tails in loop/tail mixtures becomes independent of $\sigma^{1/3}$ at relatively large σ, indicating that the chains in both sublayers impinge upon themselves within this (the scaling) regime. Self-consistent field predictions for $\langle z\rangle_S$ and $\langle z\rangle_L$ are also included (as solid lines) in *Figure 12*. These predictions, obtained from equations (8a) and (8b) with no adjustable parameters, slightly overestimate the BF simulation values for $\langle z\rangle$ of single-grafted tails in the scaling regime, but underestimate (by approximately the same amount) the simulation values for $\langle z\rangle$ of double-grafted loops in this regime. As pointed out earlier, the differences evident in *Figure 12* between the BF simulation results for loop/tail mixtures and the SCF predictions for an equivalent bidisperse tail mixture once again reflect the SCF assumption[18] of a sharp sublayer boundary (at h_S) due to complete chain demixing.

CONCLUSIONS

Bond-fluctuation simulations have been performed in this study to investigate the equilibrium conformational properties of binary mixtures of polymer loops and tails grafted to an impenetrable interface. Such mixtures are representative of physical mixtures of ordered cyclic and linear diblock copolymers of identical molecular weight[35,37], and can be used to glean insight into the layer characteristics of grafted chains possessing a second adsorbing end[41]. The segmental density distribution and layer height results obtained here reveal that the presence of tails in loop/tail mixtures serves to force the loop-rich inner sublayer to lie closer to the interface. The loops, on the other hand, force the single-grafted tails to extend (stretch) further away from the interface. The crossover from the mushroom regime (wherein the chains remain isolated and noninteracting) to the scaling regime (wherein chain impingement is responsible for lateral chain compression) appears to occur at comparable surface densities for both the loops and tails in the loop/tail mixtures examined. Simulation results for loop/tail mixtures are in favourable agreement with predictions from the self-consistent field formalism proposed by Lai and Zhulina[18] for bidisperse mixtures of grafted tails differing in length by a factor of two.

ACKNOWLEDGEMENTS

This work was supported by the Director, Office of Energy Research, Office of Basic Sciences, Chemical Sciences Division of the US Department of Energy under Contract No. DE-FG05-91ER1481 and, in part, by the donors of the Petroleum Research Fund administered by the American

Chemical Society. We would like to thank A. Halperin for valuable discussions.

REFERENCES

1. Pispas, S. and Hadjichristidis, N., *Macromolecules*, 1994, **27**, 1891.
2. Jones, R. A. L., Norton, L. J., Shull, K. R., Kramer, E. J., Felcher, G. P., Karim, A. and Fetters, L. J., *Macromolecules*, 1992, **25**, 2359.
3. Stouffer, J. M. and McCarthy, T. J., *Macromolecules*, 1988, **21**, 1204.
4. Garbassi, F., Morra, M. and Occhiello, E., in *Polymer Surfaces: From Physics to Technology*, Ch. 10. John Wiley & Sons, New York, 1994.
5. Fleer, G. J. and Scheutjens, J. M. H. M., *Coll. Surf.*, 1990, **51**, 281.
6. Zhulina, E. B., Borisov, O. V. and Priamitsyn, V. A., *J. Coll. Interface Sci.*, 1990, **137**, 495.
7. Ito, Y., in *Synthesis of Biocomposite Materials*, Ch. 1, ed. Y. Imanishi. CRC Press, Boca Raton, FL, 1992.
8. Fleer, G. J., Stuart, M. A. C., Scheutjens, J. M. H. M., Cosgrove, T. and Vincent, B., *Polymers at Interfaces*. Chapman and Hall, London, 1993.
9. Milner, S. T., *Science*, 1991, **251**, 905.
10. Mayes, A. M. and Kumar, S. K., *Mater. Res. Soc. Bull.*, 1997, **22**, 43.
11. Alexander, S., *J. Phys. II (Paris)*, 1977, **38**, 983.
12. de Gennes, P.-G., *Macromolecules*, 1980, **13**, 1070.
13. Milner, S. T., Witten, T. A. and Cates, M. E., *Macromolecules*, 1988, **21**, 2610.
14. Milner, S. T., Witten, T. A. and Cates, M. E., *Macromolecules*, 1989, **22**, 853.
15. Chakrabarti, A. and Toral, R., *Macromolecules*, 1990, **23**, 2016.
16. Birshtein, T. M., Lyatskaya, Yu.V. and Zhulina, E. B., *Polymer*, 1990, **31**, 2185.
17. Zhulina, E. B. and Birshtein, T. M., *Polymer*, 1991, **32**, 1299.
18. Lai, P.-Y. and Zhulina, E. B., *Macromolecules*, 1992, **25**, 5201.
19. Dan, N. and Tirrell, M., *Macromolecules*, 1993, **26**, 6467.
20. Murat, M. and Grest, G. S., *Macromolecules*, 1989, **22**, 4054.
21. Murat, M. and Grest, G. S., *Phys. Rev. Lett.*, 1989, **63**, 1074.
22. Murat, M. and Grest, G. S., *Macromolecules*, 1991, **24**, 704.
23. Lai, P.-Y. and Binder, K., *J. Chem. Phys.*, 1991, **95**, 9288.
24. Lai, P.-Y. and Zhulina, E. B., *J. Phys. II (France)*, 1992, **2**, 547.
25. Marko, J. F. and Chakrabarti, A., *Phys. Rev. Lett.*, 1993, **48**, 2739.
26. Vilesov, A. D., Floudas, G., Pakula, T., Melenevskaya, E. Yu., Birshtein, T. M. and Lyatskaya, Yu. V., *Macromol. Chem. Phys.*, 1994, **195**, 2317.
27. Spontak, R. J., *Macromolecules*, 1994, **27**, 6363.
28. Matsen, M. W., *J. Chem. Phys.*, 1995, **103**, 3268.
29. Spontak, R. J., Fung, J. C., Braunfeld, M. B., Sedat, J. W., Agard, D. A., Kane, L., Smith, S. D., Satkowski, M. M., Ashraf, A., Hajduk, D. A. and Gruner, S. M., *Macromolecules*, 1996, **29**, 4494.
30. Kane, L., Satkowski, M. M., Smith, S. D. and Spontak, R. J., *Macromolecules*, 1996, **29**, 8862.
31. Jones, R. L. and Spontak, R. J., *J. Chem. Phys.*, 1994, **101**, 5179.
32. Jones, R. L. and Spontak, R. J., *J. Chem. Phys.*, 1995, **103**, 5137.
33. Gulati, H. S., Hall, C. K., Jones, R. L. and Spontak, R. J., *J. Chem. Phys.*, 1996, **105**, 7712.
34. Gulati, H. S., Jones, R. L., Driscoll, D. C., Spontak, R. J. and Hall, C. K., in *Statistical Mechanics in Physics and Biology*, ed. T. C. Halsey, J. van Zanten and D. Wirtz. Mater. Res. Soc. Symp. Proc., Pittsburgh, PA, pp. 109–114.
35. Marko, J. F., *Macromolecules*, 1993, **26**, 1442.
36. Matsen, M. W. and Schick, M., *Macromolecules*, 1994, **27**, 187.
37. Lescanec, R. L., Hajduk, D. A., Kim, G. Y., Gan, Y., Yin, R., Gruner, S. M., Hogen-Esch, T. E. and Thomas, E. L., *Macromolecules*, 1995, **28**, 3485.
38. Matsen, M. W., *J. Chem. Phys.*, 1995, **102**, 3884.
39. Marko, J. F. and Witten, T. A., *Phys. Rev. Lett.*, 1991, **66**, 1541.
40. Lai, P.-Y., *J. Chem. Phys.*, 1993, **100**, 3351.
41. Skvortsov, A. M., Pavlushkov, I. V., Gorbunov, A. A. and Zhulina, E. B., *J. Chem. Phys.*, 1996, **105**, 2119.
42. Carmesin, I. and Kremer, K., *Macromolecules*, 1988, **21**, 2189.
43. Deutsch, H.-P. and Binder, K., *J. Chem. Phys.*, 1991, **94**, 2294.